Materials Advances

ROYAL SOCIETY OF CHEMISTRY

PAPER

View Article Online
View Journal

Cite this: DOI: 10.1039/d5ma01452b

Enhancing electrochromic and electrofluorochromic performance of molecular electrochromes by their covalent immobilization to nanoparticles

Mohan Raj Anthony Raj, [a] Sacha Porlier, [a] Ram Restikian [a] and W. G. Skene *[ab]

Molecular electrochromes offer the benefit of structural diversification by well-known synthetic means. However, their electrochromic performance lags behind that of their conjugated polymer counterparts. The electrochromic performance of a combined molecular electrochrome/electrofluorochrome can be enhanced by its covalent attachment to ITO nanoparticles *via* a phosphonic acid linker. A key metric of its covalent attachment to nanoparticles *via* phosphonic ester and deposition on a transparent electrode is color homogeneity over the entire electrode. This is compounded by the consistent changes in optical transmission in the NIR (890 nm) over 8 hours of switching between the colored and bleached states. Switching between the two colored states is also accelerated upwards of twofold, taking *ca.* 10 s for >85% transmission percentage difference between each state with a contrast ratio of 6. The electrofluorochromism is also improved when covalently binding the intrinsically fluorescent electrochrome to ITO nanoparticles. A high contrast ratio of 94% is obtained between the intrinsic photoemission and the quenched fluorescence upon switching the applied potential when photoexcited at 450 nm. The fluorescence on/off ratio is maintained upwards of 2 hours of reversibly applying the potential with the electrofluorochromism decaying only 18%, twofold less than in an operating electrofluorochromic device with physisorbed molecular electrochromes.

Received 12th December 2025,
Accepted 29th January 2026

DOI: 10.1039/d5ma01452b

rsc.li/materials-advances

Introduction

Phosphonic acids have garnered widespread acceptance in the field of organic electronics.[1] This is due to their capacity to modify the work function of the electrode that enables electronic devices. The covalent attachment of the acid to the transparent conductive metal oxide layer leads to a phosphonate ester–metal bond. The resulting robustly bonded monolayer can improve the device performance of organic light emitting diodes and photovoltaics. The covalent attachment of active materials with esters of phosphonic acids has also been used to improve the performance of both n- and p-type dye sensitized solar cells (DSSCs) compared to their immobilized carboxylic acid counterparts.[2,3] Indeed, the efficiency of the devices can be modulated by the alkyl chain length and the functional groups of phosphonic acid ester monolayer attached to transparent metal oxide electrodes.[4] While this approach has been readily adopted for a range of plastic electronic devices, it has been overlooked for electrochromics.[5] This field of study focuses on the reversible color change with applied potential. Electrochromic devices have found use in automotive light attenuating rearview mirrors[6] and sunroofs, smart windows for filtering sunlight,[7] privacy screens,[8] camouflage materials,[9] displays,[10] and electronic paper[11] among many other applications.

Electrochromic devices are often reliant on conjugated organic polymers. This is because they offer many advantages, including color tuning contingent on structure and being castable as films on electrodes.[12] Conjugated polymers are further electrochemically robust and can withstand extended cycles of reversibly applied potential without degradation of the bleached and colored states.[13,14] This contrasts with their molecular counterparts that undergo electrochemical reactions over time, resulting in both inconsistent coloration and device performance degradation during electrochromic device operation.[15] This aside, accurate structure/electrochromic relationships can be accurately established with molecular electrochromes.

Only recently has phosphonic acid immobilization *via* esters been leveraged with molecular electrochromes toward improving their electrochromism to match their polymer counterparts.[16] For example, conjugated ethylenedioxythiophenes were covalently

[a] *Département de chimie, Université de Montréal, Montreal, QC, Canada. E-mail: w.skene@umontreal.ca*
[b] *Institut Courtois, Université de Montréal, Montreal, QC, Canada*

attached to ITO nanoparticles *via* phosphonic acid for enhancing their electrochromic properties.[17] Zenkina *et al.* also covalently bonded a benzyl phosphonic acid to ITO.[18] This served as an anchor for covalently coupling terpyridine ligands for subsequent metal coordination, leading to a stable monolayer that changed colors between red and greenish gray over 400 cycles of applied potential with coloration efficiencies (CE) in the 100–150 $cm^2\ C^{-1}$ range. Similarly, the immobilization of the triphenylamine electrochrome and a methylviologen ion storage layer *via* phosphonic acids on the anode and cathode, respectively, enhanced the optical contrast of the operating electrochromic device.[19] Covalently immobilizing a complementary molecular electrochrome on nanostructured TiO_2 also improved the stability of the operating electrochromic device, switching between its bleached and colored states upwards of 10 000 cycles without color fatigue.[20] The performance of covalently attached molecular electrochromes is on par with other immobilization strategies that are reliant on polymers with the advantage of precise control of the molecular structure.[21–23]

The virtue of immobilizing the molecular electrochromes is that they do not diffuse from the electrode. The monomer layer therefore adheres to the electrode, resulting in rate-determining electron transfer rather than much slower mass transport.[17] This results in faster switching times between the colored states of the molecular electrochromes compared with thin films and in solution. Indeed, an optical contrast of 65% is possible and the switching between the colored states can be accelerated to 3 s during 100 cycles of switching the applied potential.[17] However, the surface coverage of a monolayer of phosphonic acid electrochrome appended to the transparent electrode is insufficient to provide visibly detectable changes that are required for most applications. ITO nanoparticles (ITO_{np}) are an emerging solution to overcome this optical limitation.[17] This is because they can be coated with a greater amount of electrochrome owing to their high aspect ratio, resulting in increased optical contrast compared to planar electrodes. Indeed, coating ITO_{np} with phosphonic acid functionalized electrochromes and their deposition on planar ITO electrodes have increased optical absorbances relative to a monolayer of electrochrome deposited uniquely on ITO transparent electrodes.[24]

Despite the advantages of phosphonic acid immobilization of electrochromes for electrochromic enhancement, the surface immobilization of electrochromes remains underexplored. **1** (Fig. 1) was prepared to provide insight into the property enhancement with the covalent attachment of the combined molecular electrochrome/electrofluorochrome to nanoparticles deposited on the transparent electrode. Of interest is the known intrinsic fluorescence of conjugated benzothiadiazoles such as **1** in solution that is carried over to the solid state.[15] This would be ideal for evaluating whether the fluorescence of a thin layer of immobilized **1** on ITO_{np} could be detected. This opens the possibility of modulating the photoinduced emission intensity with applied potential with desired large contrast ratios along with taking advantage of fast rate limited electron transfer from electrode immobilization. This is in contrast to molecular electrofluorochromes whose electrofluorochromism is limited to solution, and owing to diffusion kinetics, is extremely slow (>minutes). As such, **1** was rationally designed to be multipurpose: electrochromic, electrofluorochromic, and an intrinsic emitter. Its electrochromism and electrofluorochromism were expected to be enhanced by anchoring to ITO_{np}. Of importance, the immobilized electrochrome was expected to absorb in the NIR with applied potential. This much sought-after property for smart window applications is unprecedented for immobilized electrochromes and it would be possible to leverage it *via* the intramolecular transfer of the conjugated donor–acceptor framework. The electrochromism and electrofluorochromism of **1** immobilized on ITO_{np} and deposited as a thin layer on ITO coated glass ($\mathbf{1_{np}}$; Fig. 2) are herein presented to demonstrate that property enhancement is indeed possible by covalently anchoring conjugated molecular electrochromes to ITO_{np}. This is among the first reported examples of the covalent attachment of a conjugated donor/acceptor fluorophore to ITO_{np} for unparalleled NIR absorption along with consistent fluorescence modulation with applied potential. This serves to demonstrate that molecular fluorophores can be used as electrochromes whose performance can parallel their polymer counterparts with the advantage of precise color and fluorescence tuning by the judicious modification of molecular structure.

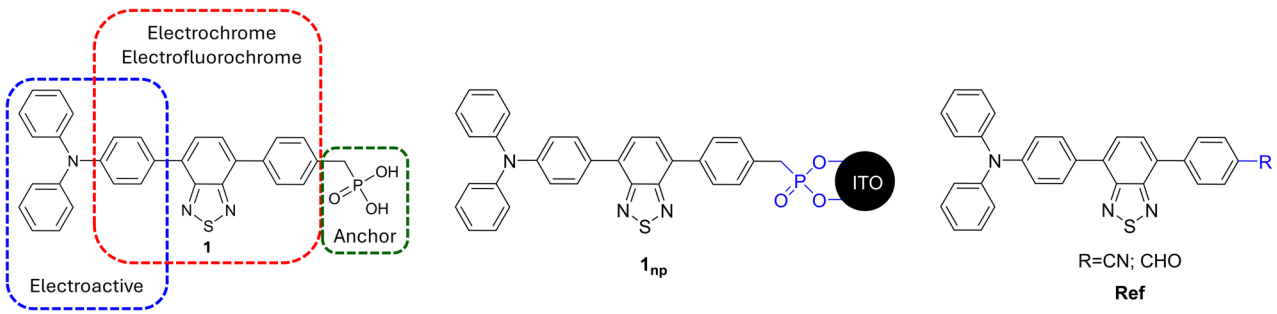

Fig. 1 Combined electrochrome/electrofluorochrome for covalent immobilization on ITO nanoparticles and deposition on ITO coated glass (**1**). Structure of the immobilized **1** on ITO nanoparticles ($\mathbf{1_{np}}$) along with the structurally equivalent reported compounds (**Ref**) for benchmarking electrochromism and electrofluorochromism.[15] Bidentate binding of **1** to an ITO nanoparticle ($\mathbf{1_{np}}$) is arbitrarily drawn to illustrate its covalent attachment.

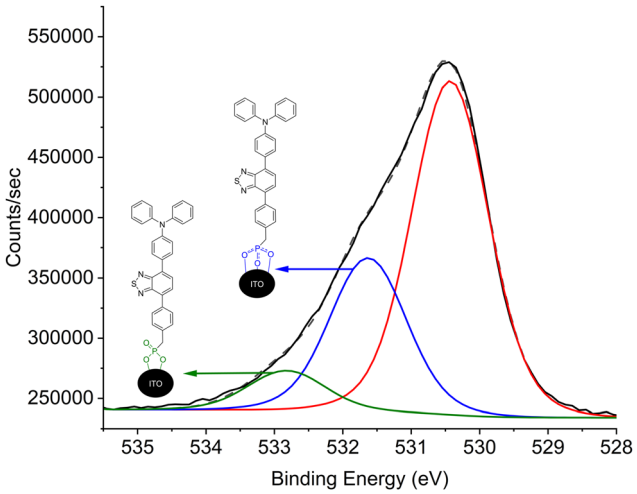

Fig. 2 XPS spectrum of the immobilized **1** on ITO_{np} ($\mathbf{1_{np}}$) and the corresponding assigned atomic oxygen. Inset: Schematic representation of the bidentate and tridentate binding of the phosphonic acid ester to ITO nanoparticles. Peaks calibrated to adventitious carbon.

Results and discussion

Preparation of combined electrochrome/electrofluorochrome

Three principal design elements were integrated into **1**. These were (1) the electroactive triphenylamine for reversible and consistent redox activity (blue line; Fig. 1) to enable the electrochromism,[25] (2) electronic push–pull conjugated framework for both absorption and emission in the visible for visually detectable electrofluorochromism (red line),[26,27] and (3) the phosphonic acid functionalization for anchoring the molecular electrochrome to ITO nanoparticles.[28] **1** was prepared as per Fig. S1 *via* a first Suzuki–Miyaura coupling of the triarylamine boronic acid with dibromobenzothiadiazole and second Suzuki–Miyaura coupling with 4-(hydroxymethyl) phenylboronic acid leading to the primary alcohol derivative which was brominated using PBr_3 to give corresponding bromo derivative. The phosphonate ester group was introduced through a Michaelis–Arbuzov reaction, followed by acid hydrolysis, yielding the final phosphonic acid derivative.[29] The identity of each product was confirmed by conventional methods.

Immobilization

The ideal method for covalently attaching the phosphonic acid to ITO_{np} was by immersing the ITO glass substrate previously coated with ITO_{np} into a solution of **1**. The equilibrium for the covalent attachment *via* the phosphonic acid with the nanoparticles is favored by a micromolar (100 μM) concentration of **1**. The physisorbed **1** was removed by rinsing the ITO_{np} coated substrate with copious amounts of ethanol. The XPS survey spectrum (Fig. S15A) of the glass substrate coated with **1** immobilized on ITO_{np} confirmed the presence of the elements C, N, O, P, and S from the electrochrome along with In and Sn from the ITO_{np} (Fig. S15 and Table S1). The P_{2p} peak was observed at 133.2 eV and it was assigned to the P-O of the phosphonic ester.[30] The degree of covalent attachment of **1** to ITO_{np} cannot be unequivocally determined exclusively from the P_{2p} peak (Fig. S16). However, its characteristic binding energy does confirm the covalent attachment of the phosphate to ITO *via* its oxygen. This is based on the absence of a deconvoluted peak at a higher binding energy (133.6 eV) that is characteristic of unbound phosphonic acid.[30] The covalent attachment of **1** to the ITO_{np} can nonetheless undoubtedly be confirmed by the deconvolution of the O_{1s} peak centered at 530.9 eV. Indeed, three distinct peaks can be deconvoluted (Fig. 2) having discrete binding energies of 532.8 (green), 531.6 (blue), and 530.4 eV (red). The peak at 531.6 eV is well known to correspond to the tridentate binding of phosphonic acid to ITO as per the inset of Fig. 2 whereas the peak at 532.8 eV is assigned to the bidentate binding. This contrasts with weakly bound phosphonic acid, whose binding energies correspond to 533.8 eV.[31] The O_{1s} peak at lower binding energies is assigned to the indium-O-indium and tin-O bonds of the nanoparticles.[32] The predominance of tridentate binding is confirmed by the 1 : 4 peak areas of the respective bi- and tridentate O_{1s} peaks. ITO_{ns}–O–P and P═O binding can be confirmed from the collective XPS data in accordance with the wealth of literature regarding the covalent attachment of phosphonic acids to ITO.[30,33–36]

The wettability of the surface was also evaluated by measuring the water contact angle of the covalently attached layer. The contact angle for the unbound surface was 20°, confirming its hydrophilicity owing to the surface hydroxyls of ITO_{np}. The contact angle increased to 110° once **1** was bound to the ITO_{np}. This increase in hydrophobicity is from the coating of hydrophobic **1** on the surface (Fig. S28). It is worthy to note that the coating of **1** on ITO_{np} was too thin for its optical evaluation by convention ATR-FTIR. The binding of **1** to ITO_{np} as per the coordination illustrated in $\mathbf{1_{np}}$ (Fig. 1) is confirmed both by XPS (Fig. 2 and Fig. S15–S19, and Table S1) and the change in surface hydrophilicity by water contact angle measurements.

Cyclic voltammetry further provided sound evidence for the covalent attachment of **1** to the working electrode. This is according to the linear correlation of current with scan rate (inset Fig. 3).[37] The linear Randles–Sevcik relationship was maintained even at slow scan rates of 20 mV s^{-1}. Physisorbed **1** would desorb at this scan rate, resulting in a significant deviation from linearity. This was indeed the case when increasing the concentration of the immersion solution to 1 mM along with the visible orange colored film. Of interest, the cyclic voltammogram of the optimized coating of **1** did not change over 10 redox cycles (Fig. S21), with the reversibility maintained even upwards of 100 redox cycles (Fig. S22). This confirmed both the chemical stability of the triphenylamine radical cation along with the persistent amount of immobilized $\mathbf{1_{np}}$. In contrast, a decrease in current would be observed for desorption of any physisorbed **1**.

Electrochromism

The performance of electrochromes (**Ref**; Fig. 1) in both solution and operating combined electrochromic and electrofluorochromic devices has been reported.[15] Given their structural similarity to **1**, they are ideal for benchmarking the

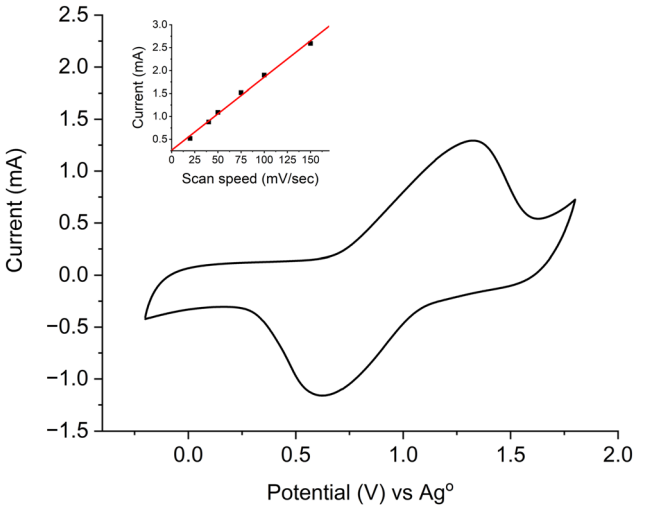

Fig. 3 Cyclic voltammogram of **1** covalently attached to ITO_{np} (**1_{np}**) coated on conductive glass measured with $LiClO_4$ (0.1 M) in propylene carbonate with a silver wire reference electrode measured at 50 mV s^{-1}. Inset: dependence of anodic peak current of **1_{np}** on electrochemical scan rate.

performance that can be enhanced by covalently attaching the electrochrome on the surface. The direct comparison of both their electrochromism and electrofluorochromism is possible given the consistent fluorophore and the common electroactive segment. Indeed, the change in absorption with applied potential was, as expected, for the immobilized **1_{np}** comparable to its as-cast physisorbed thin film counterparts. Of interest is the absorption at 890 nm in the NIR. This is ideal for preventing solar radiation transmission in smart-window applications, whether it be either architectural or automotive applications. The broad absorption from the mid-visible to the NIR (Fig. 4A) is indeed ideally suited for such applications despite the drift in the transmission baseline owing to the electrolyte. A noticeable difference between the immobilized **1** and its physisorbed counterparts is the absence of charge transfer of **1** in the NIR. This contrasts with **Ref** that have a broad absorption in the NIR centered at *ca.* 1400 nm.[15] This is a result of charge separation between the triphenylamine charge state and the terminal electronic acceptor. Given that **1** does not have an electronic acceptor, it is consistent that the NIR charge transfer does not form. This aside, an advantage of the immobilization of **1** is its consistent color of both the bleached and colored states. This is evident in the inset of Fig. 4A with the blue hue of the radical cation evenly distributed over the entire electrode.

The electrochromism provides sound evidence for the performance enhancement with the immobilization of the electrochrome. For example, the change in transmission percentage between the bleached and the blue colored states was consistent over 8 hours of continuously cycling between the two states by switching the applied potential at regular intervals. The transmission difference (Fig. 4B) decayed by only 26% during the 8 hours of switching. This result can be better appreciated by comparing the electrochromism of its structurally similar

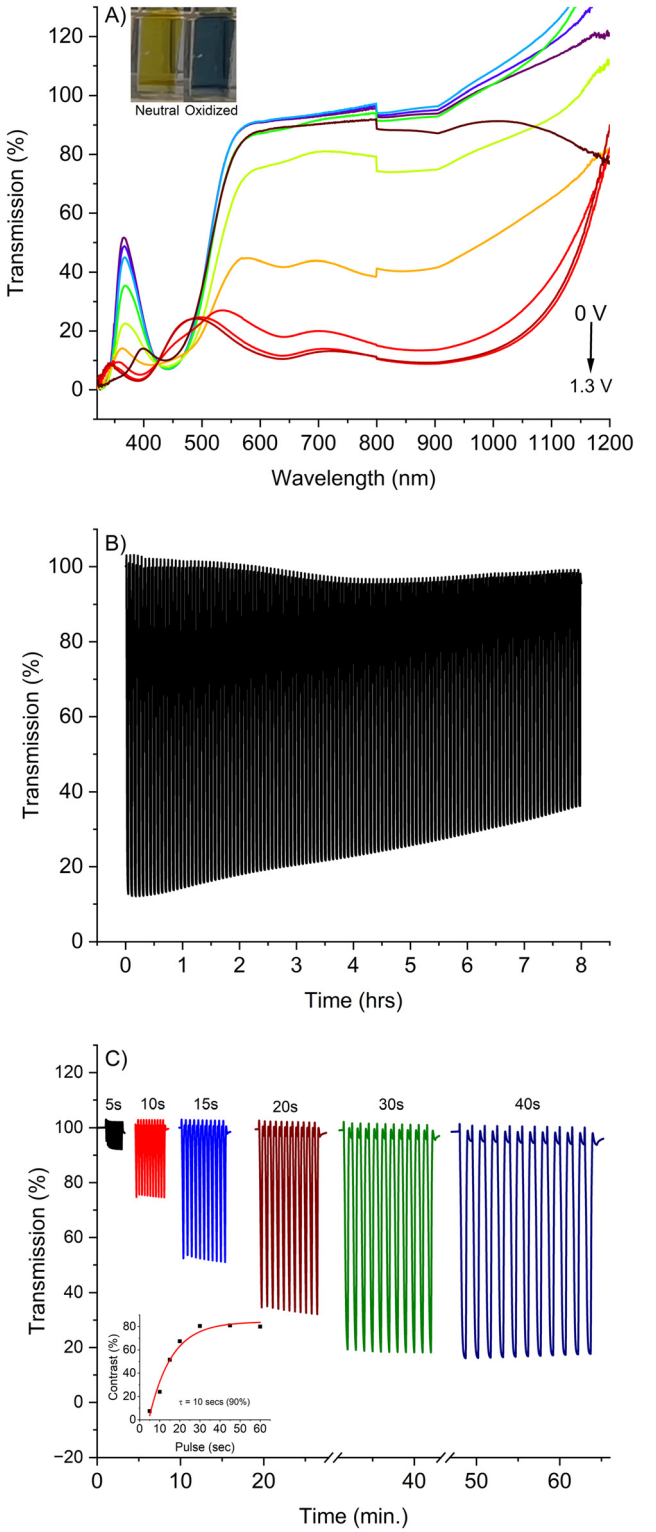

Fig. 4 (A) Transmission change of **1_{np}** with applied potential between 0 and 1.2 V measured in PC with $LiClO_4$. Inset: **1_{np}** in the neutral (left) and oxidized (right) states. (B) Change in transmission percent of **1_{np}** monitored at 890 nm with changing the applied potential between −0.2 V and 1.2 V at 2 min. intervals during 8 h. (C) Change in transmission percent of **1_{np}** monitored at 890 nm contingent on the time a potential of 1.2 V was applied. Time intervals are reported in the figure.

(**Ref**) that was deposited as a physisorbed film in an operating electrochromic device.[15] The electrochrome transmission decayed by 40% during a shorter period of time under similar cycles of switching the potential and applied potential.

The kinetics of switching between the bleached and colored states were also investigated to further illustrate the benefits of electrochrome immobilization with ITO_{np}. To better compare the kinetics between reported electrochromes and different transmission percentage differences, the universal pulse method by Padilla was used corresponding to τ = 9.9 and 5.6 s for the coloration and bleaching kinetics, respectively (Fig. S24).[38] The maximum transmission difference of 85% was obtained when applying a potential of 1.2 V, corresponding to a contrast of **1**. The bleaching and coloration kinetics graphically derived for 95% change in contrast were 10.2 and 19.2 s, respectively. These kinetics are 5–10 times slower than the fastest reported kinetics for molecular electrochromes. However, the values are faster than their structurally similar counterparts in operating devices. Indeed, they were twice as fast as physisorbed electrochromes along with color homogeneity across the entire working electrode. The kinetics are, furthermore, on par with other phosphate ester immobilized molecular electrochromes when considering the smaller transmission difference used for the switching speed measurements (Table S2). Direct comparison is possible courtesy of the universal pulse method. Coloration efficiency (CE) of the immobilized electrochrome was 150 $cm^2\ C^{-1}$, calculated by dividing the change in optical density (ΔO.D.) with charge density (Q) (Fig. S23). The coloration efficiency is lower compared to reported triphenylamines.[39–41] This can, in part, be ascribed to triphenylamines that typically undergo irreversible dimerization when electrochemically oxidized, resulting in changes in both their redox potentials and reversible coloration. This was not the case with the covalent immobilization of **1**, according to both consistent coloration and cyclic voltammograms. An ion storage cathodic material also was not used for the current study. Using such a layer is known to enhance the performance.[19,39–41] Various cathodic materials are being examined to further improve the electrochromic performance of the immobilized **1** bearing this in mind and adopting strategies that are known to bolster CE.[42–44] Nonetheless, the collective kinetic and extended switching periods between the bleached and colored states are sound evidence for the enhanced electrochromism with the covalent bonding of molecular electrochromes to the nanoparticles. The added advantage is the increased stability of the radical cation compared to physisorbed molecular electrochromes. Indeed, physisorbed triphenyl radical cations react permanently, leading to other products that change both the colored and redox states from the pristine triphenylamines.[45,46]

Electrofluorochromism

The photoemission must either be attenuated with applied potential or undergo significant changes in the emission wavelength to be considered electrofluorochromic. This was evaluated by measuring the complete emission spectrum of the immobilized fluorophore contingent on applied potential. The emission of the immobilized **1** was first benchmarked without applying the potential. Although the coating of $\mathbf{1_{np}}$ was extremely thin on the ITO_{np} that was deposited on the ITO electrode (*vide supra*), the emission could nonetheless be observed (Fig. 5). This is courtesy of the well-known solid-state emission of benzothiadiazoles.[47] The fluorescence quantum yield (Φ_{fl}) of $\mathbf{1_{np}}$ (20 nm) was 0.25% compared to Φ_{fl} = 65% for **Ref** (R = CN) in dichloromethane.[15] Two noteworthy attributes were observed with applied potential. First, the emission of $\mathbf{1_{np}}$ decreased with applied potential. This is consistent with the neutral **1** being converted to its radical cation. Secondly, the emission red-shifted and decreased with applied potential. This emission could not be quenched, either with prolonged applied potential or with increasing potential. The emission of the original $\mathbf{1_{np}}$ could be restored upon reducing the oxidized state. Similarly, the red-shifted emission could be regenerated upon oxidizing the neutral state again (Fig. S25 and S26B). To further confirm the red-shifted emission was from a unique intermediate and not from any residual neutral state, the excitation spectrum of the red-shifted emission was measured. The excitation of the

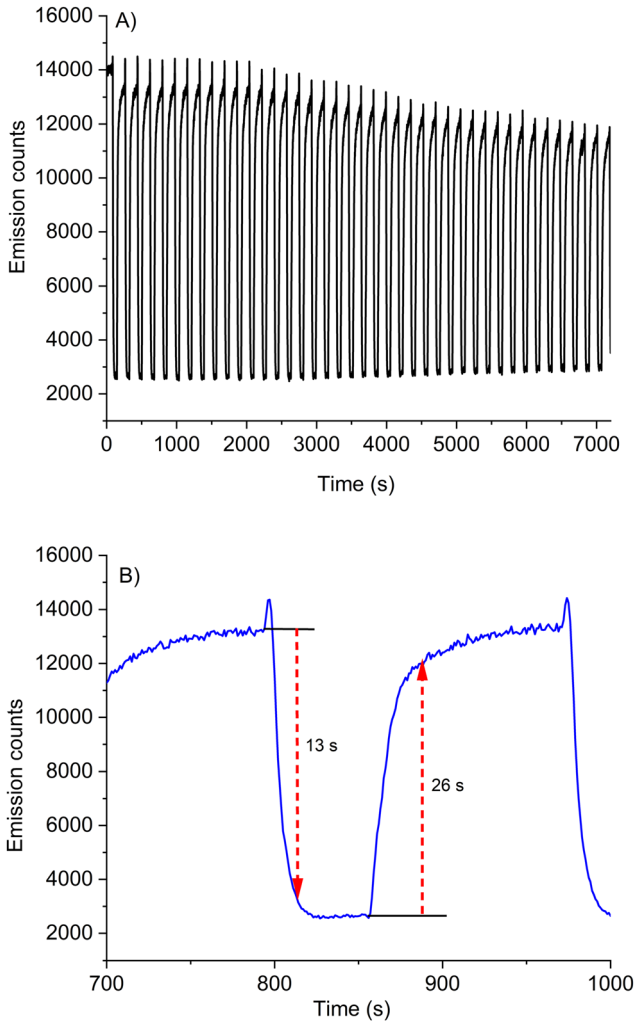

Fig. 5 (A) Change in fluorescence intensity of $\mathbf{1_{np}}$ excited and monitored at 450 nm and 600 nm, respectively, with applied potentials of 1.1 and −0.2 V switched at 1 min and 2 min intervals, respectively. (B) Expansion showing emission intensity over two potential switching events.

oxidized intermediate was quenched *ca.* fourfold relative to its neutral form. This is consistent with the decrease in absorption with applied absorption in Fig. S27A. The Φ_{fl} of the red-shifted emission was 0.27% taking into account its reduced absorption from the excitation spectrum and correcting for the emission area relative to the emission of the neutral $\mathbf{1_{np}}$ and its Φ_{fl}. The advantage of the immobilized $\mathbf{1_{np}}$ is that the red-shifted emission cannot diffuse from the surface during the measurement.

The excitation spectrum of both the neutral and charged states of $\mathbf{1_{np}}$ overlapped, precluding selective excitation of the neutral **1** and its exclusive emission. Nonetheless, the immobilized $\mathbf{1_{np}}$ was electrofluorochromic (Fig. 5A and Fig. S25, S26A). Taking into account the red-shifted residual emission, the electrofluorochromic contrast ratio was 95% based on the area of emission. This value is almost twofold greater than a structurally similar **1** whose electrofluorochromism was measured in an operating device in solution.[15] The contrast ratio is also twofold greater among the highest reported electrofluorochromes in operating devices.[48] Although direct comparison of structurally different electrochromes should be avoided because of differences in intrinsic emission, the contrast ratio is nonetheless improved with the immobilization of the electrochrome on the electrode.

There are many major challenges that limit electrofluorochromism, one such being the change in photoexcited emission with applied potential. On one hand, the fluorophore must appreciably emit in the solid state, especially when cast as a thin film. Conjugated benzothiadiazoles such as **1** are ideal because of their intrinsic high emission yield that is carried over to the solid state. This is indeed the case with triphenylamine benzothiadiazoles of **1**.[29] On the other hand, the fluorophore must be immobilized on the electrode for a maximum change in the contrast ratio. This is because all of the immobilized fluorophores can be rapidly converted to their redox state. This contrasts with when the fluorophore is soluble and it must continuously diffuse to the electrode to generate its redox state. This requires long periods of applied potential to deplete the fluorophore. Indeed, the emission on/off kinetics in Fig. 5B is faster than those for the structurally similar **Ref** in an operating combined electrochromic/electrofluorochromic device. The coloration time to quench the emission was fourfold faster and bleaching time to recover the emission was 2–3 times faster with $\mathbf{1_{np}}$ compared to its unbound counterpart **1** when measured in diffused controlled solution.[15] Also, the contrast ratio decreased by 26% with continuous operation of switching the applied potential between the fluorescence on/off states at regular intervals. These data provide sound evidence for enhancing the electrofluorochromic performance, including accelerated kinetics and consistent coloration, by the covalent immobilization of the molecular electrochrome to the electrode in contrast to its physisorption as a thin film layer in operating devices.

Conclusions

Immobilization of a combined molecular electrochrome and electrofluorochrome *via* a phosphonic acid ester to ITO nanoparticles improved its overall performance. Indeed, many gains in the electrochromism are obtained by covalently attaching electrochromes in comparison to their physisorbed counterparts. These include consistency in the colored and bleached states over extended periods of electrochemical cycling between the two states, improved stability of the electrochemical mediated state, and uniform coloration over the entire surface. Of importance, immobilization of the electrochrome prevents diffusion, resulting in improved kinetics of switching between the two colored states. Moreover, preventing diffusion enhances the electrofluorochromism along with ensuring consistent contrast ratios even during prolonged electrochemical switching between the two states. The electrochromic and electrofluorochromic performance of molecular electrochromes can be improved by covalently attaching them to the electrode with metrics reaching those of their polymer counterparts. Given the well-developed means of integrating phosphonic acids and their covalent attachment to ITO nanoparticles taken together with the tuneable colored states possible by judiciously modifying the molecular structure, molecular electrochromes are emerging as viable materials for achieving control and selected colors for operating devices.

Conflicts of interest

The authors declare no conflict of interest.

Data availability

The data supporting the findings are presented in the manuscript and the supporting information (SI). Supplementary information: NMR, XPS, spectroelectrochemical, emission, and electrofluorochromic spectra along with cyclic voltammograms and synthetic details. See DOI: https://doi.org/10.1039/d5ma01452b.

Acknowledgements

NSERC Canada and the Canada Foundation for Innovation are thanked for operating and infrastructure grants, respectively, which supported this work. Dr L. Shang is thanked for assistance with the XPS measurements. N. Chelfouh is acknowledged for assistance with doctor blading. The Quebec Center for Advanced Materials (QCAM/CQMF) is also acknowledged for providing access to equipment and resources that supported this work along with the Institut Courtois.

References

1 K. Kalyanasundaram and M. Grätzel, *Coord. Chem. Rev.*, 1998, **177**, 347–414.
2 A. Abate, R. Pérez-Tejada, K. Wojciechowski, J. M. Foster, A. Sadhanala, U. Steiner, H. J. Snaith, S. Franco and J. Orduna, *Phys. Chem. Chem. Phys.*, 2015, **17**, 18780–18789.
3 Y. M. Klein, N. Marinakis, E. C. Constable and C. E. Housecroft, *Crystals*, 2018, **8**, 389.

4 R. Stalder, D. Xie, A. Islam, L. Han, J. R. Reynolds and K. S. Schanze, *ACS Appl. Mater. Interfaces*, 2014, **6**, 8715–8722.
5 M. R. Anthony Raj, H. V. Humeniuk and W. G. Skene, *ChemPlusChem*, 2025, **90**, e202500178.
6 H. N. Kim, S. M. Cho, C. S. Ah, J. Song, H. Ryu, Y. H. Kim and T.-Y. Kim, *Mater. Res. Bull.*, 2016, **82**, 16–21.
7 Z. Zhou, Y. Fang, X. Wang, E. Yang, R. Liu, X. Zhou, Z. Huang, H. Yin, J. Zhou and B. Hu, *Nano Energy*, 2022, **93**, 106865.
8 S. Wu, H. Sun, M. Duan, H. Mao, Y. Wu, H. Zhao and B. Lin, *Cell Rep. Phys. Sci.*, 2023, **4**, 101370.
9 H. Fu, L. Zhang, Y. Dong, C. Zhang and W. Li, *Mater. Chem. Front.*, 2023, **7**, 2337–2358.
10 C. J. Gu, A.-B. Jia, Y.-M. Zhang and S. X.-A. Zhang, *Chem. Rev.*, 2022, **122**, 14679–14721.
11 D. Corr, U. Bach, D. Fay, M. Kinsella, C. McAtamney, F. O'Reilly, S. N. Rao and N. Stobie, *Solid State Ionics*, 2003, **165**, 315–321.
12 D. Chen, Z. Tong, Q. Rao, X. Liu, H. Meng and W. Huang, *Nat. Commun.*, 2024, **15**, 8457.
13 P. M. Beaujuge and J. R. Reynolds, *Chem. Rev.*, 2010, **110**, 268–320.
14 L. Brändler, L. Niklaus, P. Löbmann, M. Schott and G. A. Giffin, *Adv. Mater. Technol.*, 2025, **10**, 70018.
15 M. R. A. Raj, C. Yao, G. Balakrishnan Muthuperumal, L. Hu, A. Malinge, M. Frémont, C. Cambe, O. Ortiz, S. Porlier and W. G. Skene, *ChemPlusChem*, 2025, **90**, e202400667.
16 K. E. Johnson, D. E. Shen, J. R. Reynolds and A. L. Dyer, *Polym. Adv. Technol.*, 2024, **35**, e6551.
17 A. M. Österholm, L. Nhon, D. E. Shen, A. M. Dejneka, A. L. Tomlinson and J. R. Reynolds, *Mater. Horiz.*, 2022, **9**, 252–260.
18 J. T. S. Allan, S. Quaranta, I. I. Ebralidze, J. G. Egan, J. Poisson, N. O. Laschuk, F. Gaspari, E. B. Easton and O. V. Zenkina, *ACS Appl. Mater. Interfaces*, 2017, **9**, 40438–40445.
19 M. Li, Y. Wei, J. Zheng, D. Zhu and C. Xu, *Org. Electron.*, 2014, **15**, 428–434.
20 D. Cummins, G. Boschloo, M. Ryan, D. Corr, S. N. Rao and D. Fitzmaurice, *J. Phys. Chem. B*, 2000, **104**, 11449–11459.
21 C.-H. Du, Y.-H. Xu, H. Li, Z.-X. Wu, H.-J. Yang, X.-M. Liu, B.-Y. Lu, G.-M. Nie and G. Zhang, *Chin. J. Polym. Sci.*, 2024, **42**, 1749–1757.
22 D. Yu, E. Jang, Y. Wi, J. Hyeong, K. M. Lee, N. P. Godman, M. E. McConney, L. De Sio, S.-I. Lim and K.-U. Jeong, *Adv. Funct. Mater.*, 2025, **35**, 2420062.
23 K. Zhai, Q. Fan, Z. Bai, B. Bao, X. Wu, Q. Zhang, Y. Li, C. Hou, K. Li and H. Wang, *Adv. Funct. Mater.*, 2024, **34**, 2404029.
24 D. E. Shen, D. B. Iyer, A. M. Dejneka, J. R. Reynolds and A. M. Österholm, *ACS Appl. Opt. Mater.*, 2023, **1**, 906–914.
25 H.-J. Yen, Y.-R. Kung, S.-H. Hsiao and G.-S. Liou, in *Electrochromic Smart Materials: Fabrication and Applications*, ed. J. W. Xu, M. H. Chua and K. W. Shah, The Royal Society of Chemistry, 2019, ch. 11, pp. 323–371, DOI: 10.1039/9781788016667-00323.
26 B. A. D. Neto, P. H. P. R. Carvalho and J. R. Correa, *Acc. Chem. Res.*, 2015, **48**, 1560–1569.
27 B. A. D. Neto, A. A. M. Lapis, E. N. da Silva Júnior and J. Dupont, *Eur. J. Org. Chem.*, 2013, 228–255.
28 S. A. Paniagua, A. J. Giordano, O. N. L. Smith, S. Barlow, H. Li, N. R. Armstrong, J. E. Pemberton, J.-L. Brédas, D. Ginger and S. R. Marder, *Chem. Rev.*, 2016, **116**, 7117–7158.
29 S. Kato, T. Matsumoto, M. Shigeiwa, H. Gorohmaru, S. Maeda, T. Ishi-i and S. Mataka, *Chemistry*, 2006, **12**, 2303–2317.
30 J. Köbl, D. Wechsler, E. Y. Kataev, F. J. Williams, N. Tsud, S. Franchi, H.-P. Steinrück and O. Lytken, *Surf. Sci.*, 2020, **698**, 121612.
31 C. Zhang, S. Das, N. Sakurai, T. Imaizumi, S. Sanjayan, Y. Shoji, T. Fukushima and M. Zharnikov, *Phys. Chem. Chem. Phys.*, 2024, **26**, 11360–11369.
32 W. Zhang, W. Ju, X. Wu, Y. Wang, Q. Wang, H. Zhou, S. Wang and C. Hu, *Appl. Surf. Sci.*, 2016, **367**, 542–551.
33 P. B. Paramonov, S. A. Paniagua, P. J. Hotchkiss, S. C. Jones, N. R. Armstrong, S. R. Marder and J.-L. Brédas, *Chem. Mater.*, 2008, **20**, 5131–5133.
34 W.-C. Lan, T.-S. Huang, Y.-C. Cho, Y.-T. Huang, C. J. Walinski, P.-C. Chiang, M. Rusilin, F.-T. Pai, C.-C. Huang and M.-S. Huang, *Appl. Sci.*, 2020, **10**, 590.
35 S. A. Paniagua, E. L. Li and S. R. Marder, *Phys. Chem. Chem. Phys.*, 2014, **16**, 2874–2881.
36 K. Magra, J.-F. Audibert, D. Dragoe, T. Mallah, F. Miomandre and M.-L. Boillot, *Adv. Opt. Mater.*, 2023, **11**, 2301128.
37 J. Wang, *Analytical Electrochemistry*, Wiley-VCH, 3rd edn, 2006.
38 S. Hassab, D. E. Shen, A. M. Österholm, M. Da Rocha, G. Song, Y. Alesanco, A. Viñuales, A. Rougier, J. R. Reynolds and J. Padilla, *Sol. Energy Mater. Sol. Cells*, 2018, **185**, 54–60.
39 D. Weng, Y. Shi, J. Zheng and C. Xu, *Org. Electron.*, 2016, **34**, 139–145.
40 C. Kortz, A. Hein, M. Ciobanu, L. Walder and E. Oesterschulze, *Nat. Commun.*, 2019, **10**, 4874.
41 M. Ciobanu, J. Klein, M. Middendorf, S. M. Beladi Mousavi, F. Carl, M. Haase and L. Walder, *Sol. Energy Mater. Sol. Cells*, 2019, **203**, 110186.
42 D. Liu, N. Li, Q. Fan, W. Liu, Y. Zhang, L. Xu, J. Zhao, L. Zhang and Y. Li, *Chem. Eng. J.*, 2025, **526**, 170665.
43 X. Luo, R. Wan, Z. Zhang, M. Song, L. Yan, J. Xu, H. Yang and B. Lu, *Adv. Sci.*, 2024, **11**, 2404679.
44 Z. Wu, Q. Zhao, X. Luo, H. Ma, W. Zheng, J. Yu, Z. Zhang, K. Zhang, K. Qu, R. Yang, N. Jian, J. Hou, X. Liu, J. Xu and B. Lu, *Chem. Mater.*, 2022, **34**, 9923–9933.
45 O. Yurchenko, D. Freytag, L. zur Borg, R. Zentel, J. Heinze and S. Ludwigs, *J. Phys. Chem. B*, 2012, **116**, 30–39.
46 P. Blanchard, C. Malacrida, C. Cabanetos, J. Roncali and S. Ludwigs, *Polym. Int.*, 2019, **68**, 589–606.
47 Y. Zhang, J. Song, J. Qu, P.-C. Qian and W.-Y. Wong, *Sci. China Chem.*, 2021, **64**, 341–357.
48 A. N. Woodward, J. M. Kolesar, S. R. Hall, N.-A. Saleh, D. S. Jones and M. G. Walter, *J. Am. Chem. Soc.*, 2017, **139**, 8467–8473.